ILD-NOTE-2019-XXX

Heavy Flavour Benchmarks of ILD

Abstract

An overview of the performance of the ILD detector in its version Large and Small as relevant for the IDR is given

Contents

1. Introduction

It has been shown in recent publications that heavy quarks may be important messengers of new physics. High precision e^+e^- collisions with polarised beams around the TeV scale are ideally suited to detect new physics effects. The detection of the onset of new physics require however a superb detector performance in terms of flavor tagging including the event by event determination of the charge of the final state jets. The charge determination happens mainly by a combination of the determination of the summed charge of tracks pointing to a secondary vertex or by the identification of the charge of a final state Kaon. This is turn requires a successful particle identification by the detector. Therefore processes with heavy quark final states, i.e. $e^+e^- \to b\bar{b}$ and $e^+e^- \to t\bar{t}$ are highly relevant for the benchmarking of the detector performance. In short one can test the following detector capacities.

- Track finding efficiency
- Stringent test of (secondary) vertexing
- Particle ID
- In case of $e^+e^- \to t\bar{t}$ leptonic and semi-leptonic decays of the top-quark pair provide an important additional handle for the accurate measurement of the final state. The analysis presented in this note focuses on the semi-leptonic decay mode of the top-quark pair.

The analyses presented in this note start out from the PhD thesis of Sviatoslav Bilokin that are based on the DBD samples and software versions. This work has in part been published as arxiv:1709.xxxx. The analyses are ported to the large and small detector models and are carried out with the software version that is relevant for the IDR of ILD. For the process $e^+e^- \to b\bar{b}$ an analysis at $\sqrt{s} = 500\,\mathrm{GeV}$ is presented instead of $\sqrt{s} = 250\,\mathrm{GeV}$ as in Refs.. The results also benefit from a refined analysis strategy for the ILD paper that is under review in ILD.

2. Methods, tools and Monte Carlo samples

For the event reconstruction we use the `ILCSoft` version `v02-00-02` We use the following methods

- 'Core tools'
  - We use the `ValenciaVertex` jet algorithm implemented in `LCFIPlus` that provides the rejection of $\gamma\gamma$ background. In this algorithm the distance between two objects is calculated as
$$d_{ij} = 2\min(E_i^{2\beta}, E_j^{2\beta})(1 - \cos\theta_{ij})/R^2 \tag{1}$$
    The distance of a particle i to the beam is calculated according to.
$$d_{iB} = E^{2\beta}\sin^{2\gamma}\theta_{iB} \tag{2}$$
    The jet algorithm is run with the following settings: $\alpha = \beta = \gamma = 1$, $R = 1.4$
  - We use the `LeptonFinder` in case of semi-leptonic $e^+e^- \to t\bar{t}$ events
  - For the vertex finding we use the `LCFIPlus` version v.xxxx. QUESTION: DO WE USE THE REPROCESSED SAMPLES BY RYO?
- Tools developed for the study
  - The `VertexRestorer` Processor identifies tracks that have not been associated to secondary vertices from B-Meson decays but belongs to this decay according to the Monte Carlo Truth information. It then recovers the 'lost' tracks by means of the impact parameters d_0 (transversal) and z_0 (longitundinal). In this present note the recovery uses only the impact parameter d_0 since the algorithms needs to be adapted for the vertex smearing present in the simulation for the IDR.
  - The `ParticleTagger` Processor identifies the Kaons by means of the dE/dx measured in the TPC of ILD. It selects a strip in the dE/dx-momentum plane with a high kaon concentration. The efficiency and the purity of the Kaon selection vary as a function of the width of this strip.
  - The `QQbarAnalysis` Processor calculates the jet charge and the polar angle of the bottom and top quark pair, respectively. It contains separate methods for the bottom and top quark pair analysis.
  - The `TrashRecoProcessor` enables comparisons between reconstructed and generated quantities.
  - The described tools are available under https://github.com/QQbarAnalysis. This repository contains also a set of macros necessary for the final steps of the analysis.
- Quark charge measurement and corrections for miscalculations
  - Probabilities on double charge measurements for $t\bar{t}$ and $b\bar{b}$ has been examined.

– Calculations scheme is shown below.

$$\left.\begin{aligned} N_{acc} &= Np^2 + Nq^2 \\ N_{rej} &= 2Npq \\ 1 &= p + q \end{aligned}\right\} \quad N_{corr} = N_{acc} \cdot \frac{p^2}{p^2+q^2} \tag{3}$$

– where N is total number of events, N_{acc} and N_{rej} are number of events that were accepted and rejected, respectively. p and q values represents probabilities of events being accepted and rejected. Solving this equation will give us back both p and q, thus improving our results on A_{fb}.

– the correction has been applied to the $b\bar{b}$ studies while not in $t\bar{t}$. Selection scheme in $t\bar{t}$ is much more complicated than that for $b\bar{b}$ thus applying the correction will reduce the efficiency with little effect.

2.1. Monte Carlo samples and Event processing

For this benchmark study only processes with *left-handed* electron polarisation and *right-handed* positron polarisation have been studied so far. The final states resulting from this configuration are more demanding for the detector performance in terms of the control of migration effects.

More precisely the results presented in this note are based on the following samples:

- $e^+e^- \to t\bar{t}$:
  - $yyxye\nu$: https://ild.ngt.ndu.ac.jp/elog/opt-data/?GenProcessID=108670
    This sample contains the final state resulting from the $W \to e\nu$ decay. The generated cross section is 116.9 fb and the total integrated luminosity is about 2200 fb^{-1}. CHECK EVENT NUMBERS!!!
  - $yyxyl\nu$: https://ild.ngt.ndu.ac.jp/elog/opt-data/?GenProcessID=108675.
    This sample contains the final state resulting from the $W \to \ell\nu$ decay with $\ell = \mu, \tau$. The generated cross section is 213.25 fb and the total integrated luminosity is about 2100 fb^{-1}. CHECK EVENT NUMBERS. For the analysis presented here the final state with $\ell = \tau$ has been discarded.
- $e^+e^- \to b\bar{b}$: https://ild.ngt.ndu.ac.jp/elog/opt-data/?GenProcessID=250114 The generated cross section is 32470 fb and the total integrated luminosity is about 46 fb^{-1}

In both cases the samples available for small and large detectors are available and comparisons will be presented where appropriate.

3. Efficiencies and Control plots

The Figs. 1 and 2 show the missed tracks before and after vertex recovery for the $e^+e^- \to b\bar{b}$ and $e^+e^- \to t\bar{t}$ analyses, respectively. Both figures suggest a systematic improvement in the assignment of secondary vertices. This improvement is quantified in Figs. 3 and 4 where the purity of the b-charge reconstruction is shown as a function of the $b - tag$ valaue, the reconstructed b-momentum $|p_{had}|$ the number of reconstructed tracks assigned to a secondary vertex N_{rec} and finally the polar angle of the b-hadron. here denoted as $|\cos\theta|$. The improvemt is is larger for the process $e^+e^- \to t\bar{t}$ than for $e^+e^- \to b\bar{b}$. Qualitatively this is expected since the tracks produced in the decay of the b-hadron are softer in case of top-pair production. In case of $e^+e^- \to t\bar{t}$ the improvemnt is 10% over a large range in $|\cos\theta|$ and mainly driven by three to five prong decays. Both results will further improve once the vertex recovery takes also the the impact parameter z_0 into account. All results shown so far in this section have been obtained for the large detector model. The conclusions for the small detector model are similar.

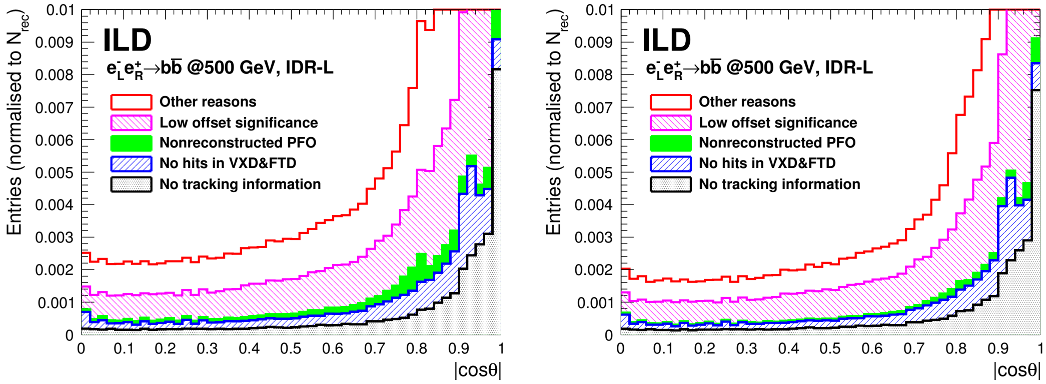

Figure 1: *Vertex recovery in case of the $e^+e^- \to b\bar{b}$ process.*

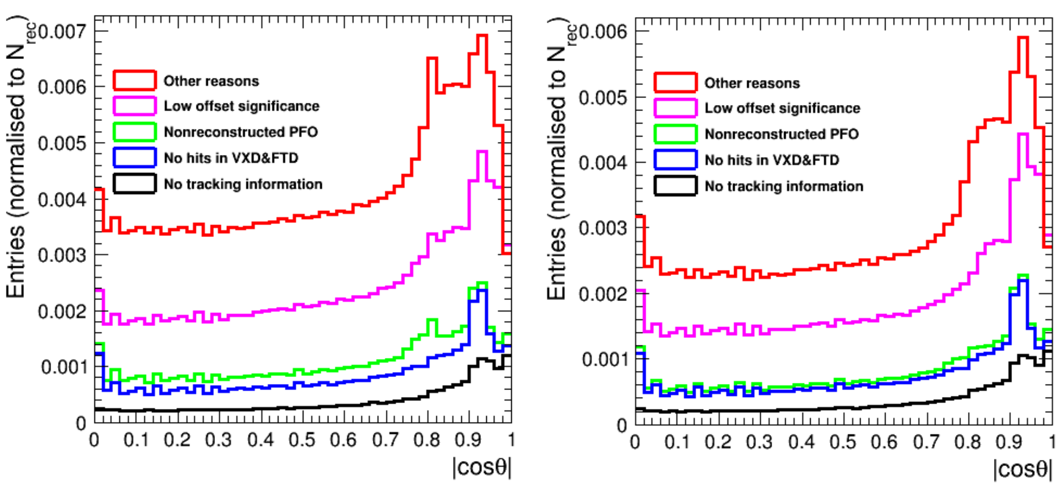

Figure 2: *Vertex recovery in case of the $e^+e^- \to t\bar{t}$ process.*

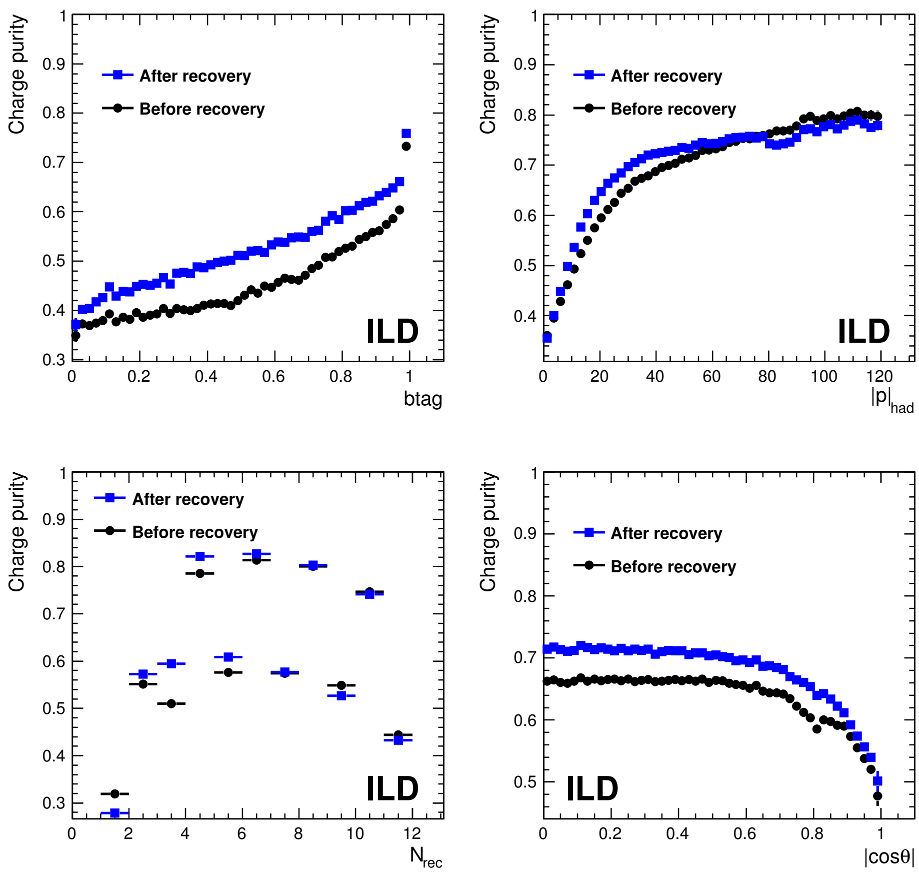

Figure 3: *Purity before and after vertex recovery in case of the $e^+e^- \to b\bar{b}$ process for different observables.*

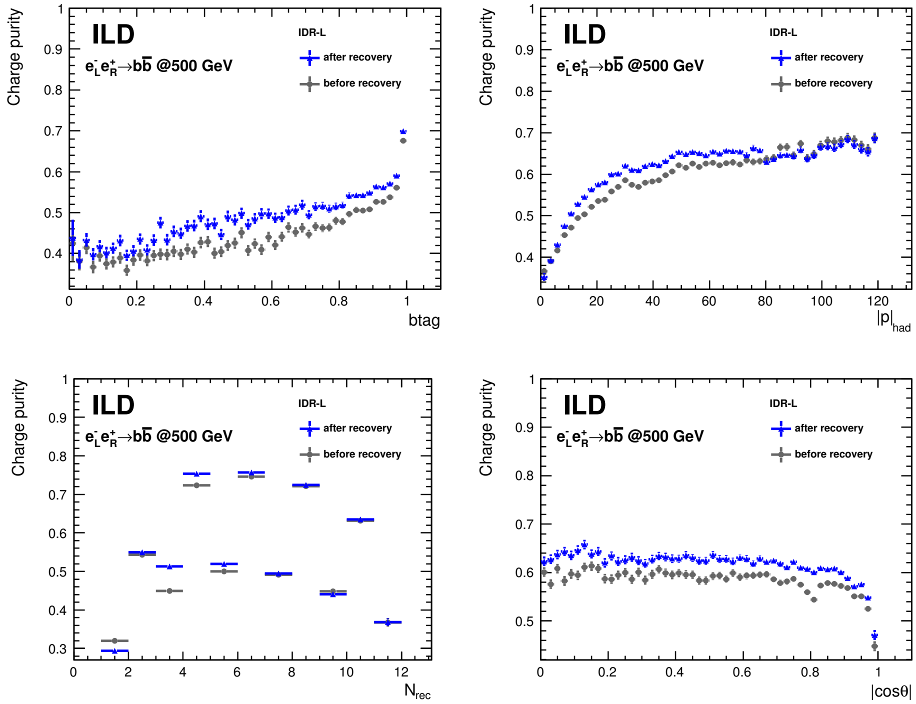

Figure 4: *Purity before and after vertex recovery in case of the $e^+e^- \to t\bar{t}$ process for different observables.*

The lower right panels of Figs. 3 and 4 show a drop in purity for large values of $|\cos\theta|$. This is compatible with the drop in acceptance that is shown in Fig. 5 for the case $e^+e^- \to b\bar{b}$ as a function of the plolar angle of the reconstructed b-jet $|\cos\theta_b|$. Within statistical errors the results are the same for the large and the small detector model. However, towards large values of $|\cos\theta_b|$ the large detector performs systematically better than the small detector.

A component that distinguishes the ILD Detector from other proposals for e^+e^- colliders is the TPC as the central tracking system. Beside the precise momentum measurement the dE/dx measurement in the gaseous medium allows for a particle identification. Since around 80% of B-Mesons (neutral or charged) contain a charged Kaon among their decay products the particle ID can support greatly the charge determination of the b-quark. The Fig. 6 displays the normalised dE/dx spectrum for different particles in different momentum ranges for the large and the small detector model. In both cases there is a clear separation of Kaons from pions. The latter are however much more abundant. There is only a small population of protons. Figure 7 shows the dE/dx spectra for the two processes under study. Finally the Fig. 8 shows the variation of the purity as as a function of the Kaon selection efficiency.

4. Analysis details specific to bb analysis

Table 1 shows the selection efficiencies for the $e^-_L e^+_R \to b\bar{b}$ analysis. The overall efficiency is with around 64% to 65% similar for both detector models. For the b-charge measurement opposite charges in opposite jets are required. The charges are either derived from the tracks pointing to the secondary vertex or from the Kaon charge or from a combination of both. The efficiencies for the different methods are given in Tab. 2. The purity of the different methods is shown in Fig. 9 . In both cases there is no large difference between the two detector models although the large detector seem to perform slightly better for the double Kaon method.

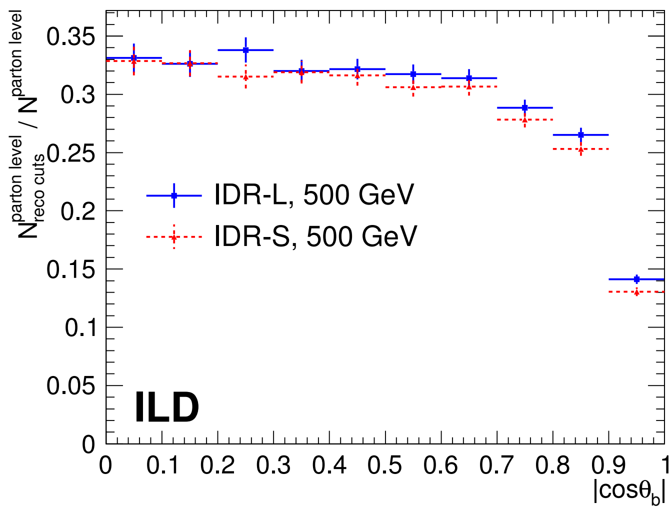

Figure 5: Detector acceptance distribution for b-tagged jets. WHY IS THERE A PLATEAU AT 0.32? TAB 1 REPORTS AN OVERALL EFFICIENCY OF 64 - 65%%

$e^-_L e^+_R \to b\bar{b}$ at 500 GeV

	IDR-L			IDR-S		
	Signal	$B_{b\bar{b}}$/S	$B_{rad.Z}$/S	Signal	$B_{b\bar{b}}$/S	$B_{rad.Z}$/S
Full sample	100.0%	1800.5%	359.1%	100.0%	1800.6%	359.0%
$b_{tag}(jet_1) > 0.9$ and $b_{tag}(jet_2) > 0.2$	70.2%	2.3%	147.7%	69.9%	2.3%	149.0%
$m_{jet_1+jet_2} > 200GeV$	68.2%	1.4%	6.7%	67.8%	1.2%	6.7%
$E_{photon} < 100GeV$	64.8%	1.3%	1.7%	64.3%	1.2%	1.6%

Table 1: Selection efficiency and B/S rejection for some bkg sources

5. Analysis details specific to tt-analysis

- Energy and polar angle spectrum of selected isolated lepton MISSING
- Table with selection efficiencies MISSING OR BETTER INCOMPLETE
- For the record we may add the observation by Amjad on the b/c tagging.

Figure 10 shows the fraction of accepted events, see Eq. 2 for different methods used to distinguish the top from the anti-top.

Table 4 shows the overall selection efficiencies and the generated and reconstructed value of the forward-backward asymmetry A_{FB} as an estimator for the quality of the reconstruction.

6. Results

Figure 11 shows the polar angle spectrum after the application of Eq. 2 for the $e^-_L e^+_R \to b\bar{b}$. Large and small detector agree within statistical uncertainties. It seems however that there is larger migration for the small detector.

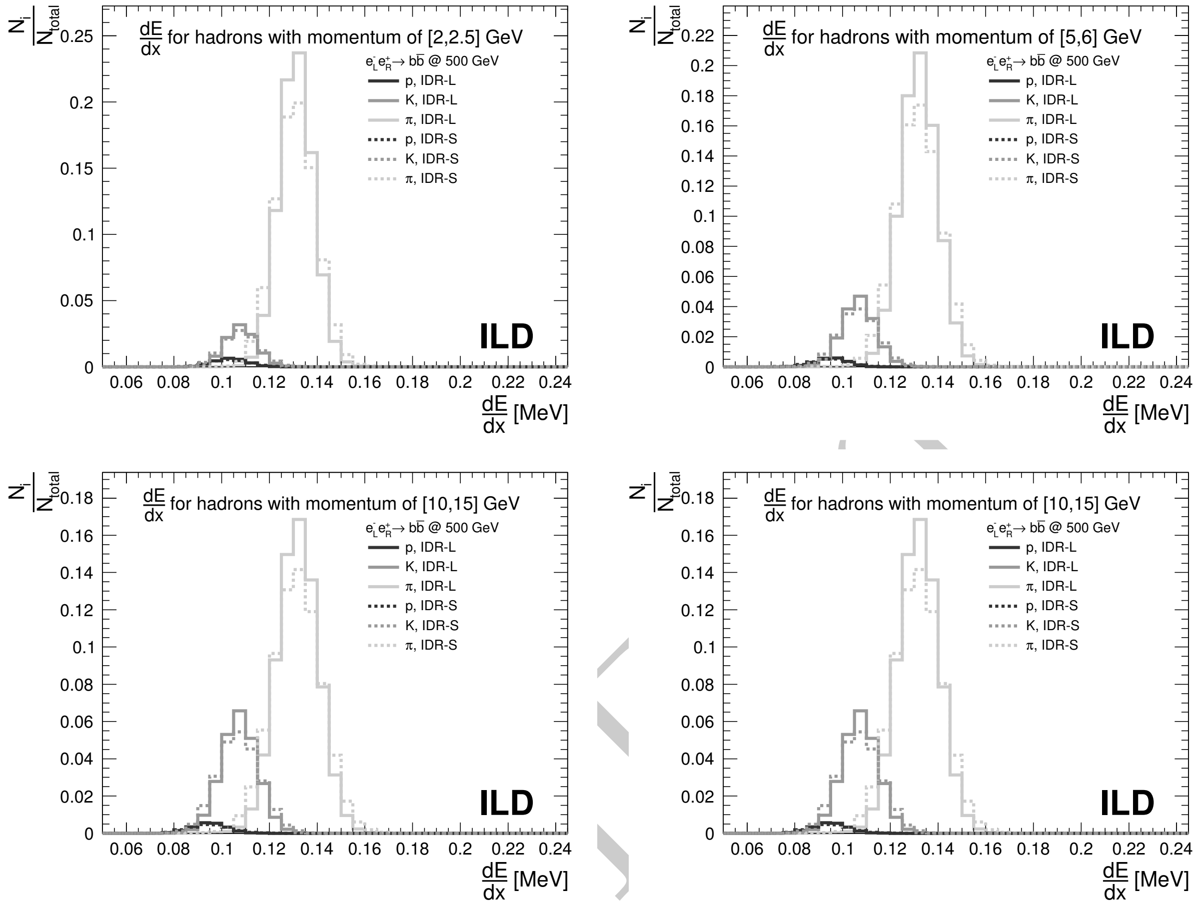

Figure 6: Projection of dE/dx for several momentum ranges. Comparison of hadron separation performance by different detector models in $b\bar{b}$ final states.

The left part of Fig. 12 shows the polar angle distribution of $t\bar{t}$ of the generated and reconstructed data for the large and the small detector models. The red dotted line shows the fitted result of the reconstructed events. The right part shows the polar angle distribution of the underlying b-quark.

7. Summary

SUMMARY FROM BBBAR ANALYSIS TO BE ADDED.

No significant differences were confirmed between s5 and l5 samples. For the $t\bar{t}$ studies, we see that the polar angle distribution is consistent with the Parton level result. At the edges of the polar angles, we do not see inefficiencies due to the detector geometry. Inefficiencies of at the edges of the detectors originates from inability to reconstruct b jets going to the forward region. For the top pair reconstruction, we can also rely on W informations thus not losing much efficiencies at the edges.

Acknowledgements

References

Appendix

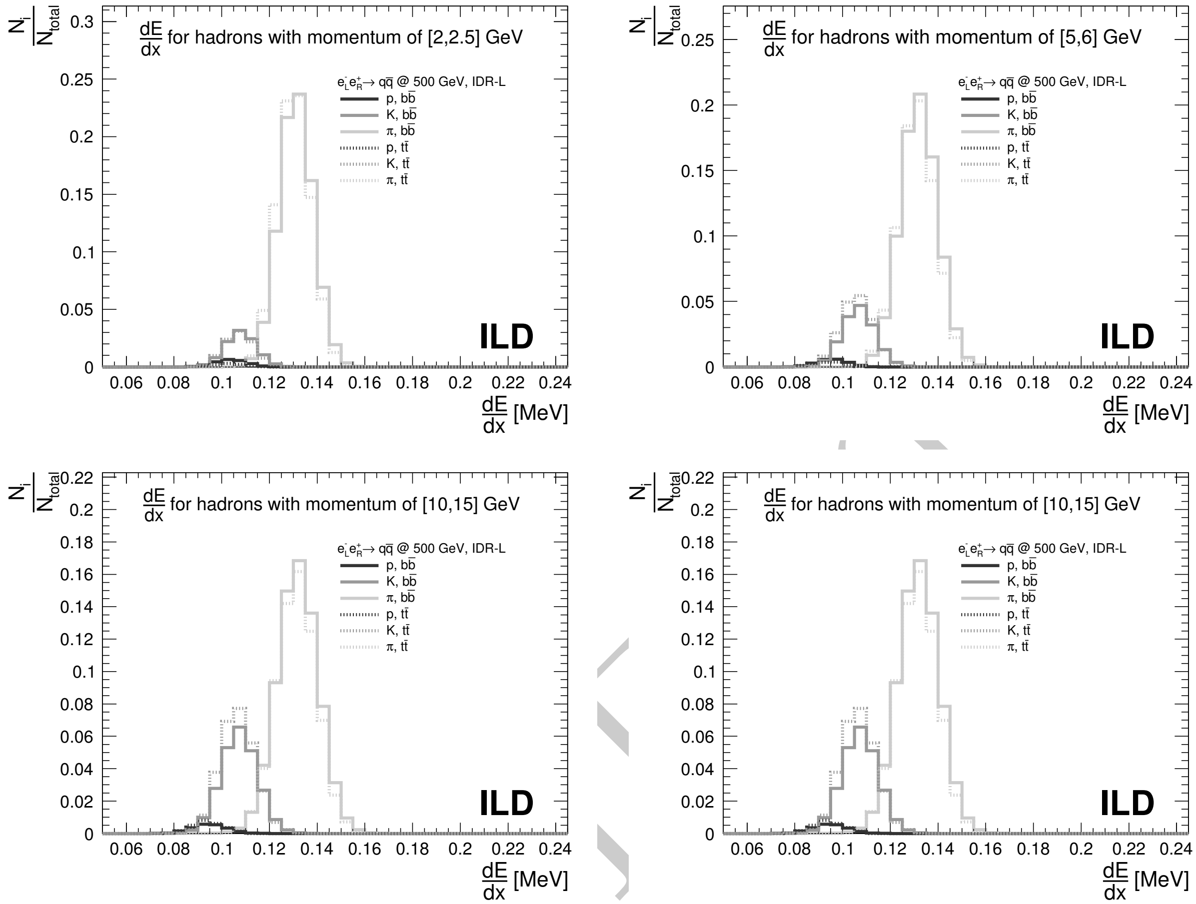

Figure 7: Projection of dE/dx for several momentum ranges. Comparison of hadron separation performance by the large model for different topologies.

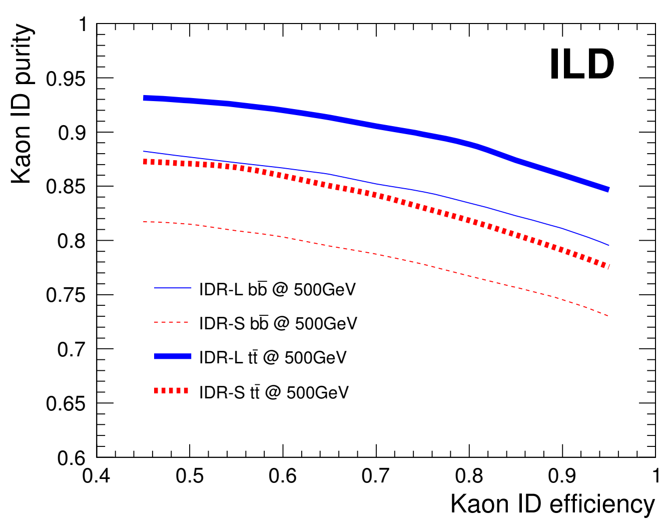

Figure 8: QUESTION: ARE THE DIFFERENT VALUES OF PURITY AND EFFICIENCY DUE TO A VARIATION OF THE STRIP IN THE DE/DX-MOMENTUM PLANE?

$e^-_L e^+_R \rightarrow b\bar{b}$ at 500 GeV

	IDR-L	IDR-S
Vtx+Vtx	12.9%	12.8%
K+K	4.4%	4.0%
Vtx+K (diff. jets)	3.9%	3.7%
Vtx+K (same jet)	7.7%	7.4%

Table 2: Final selection efficiency, after double jet-charge measurement

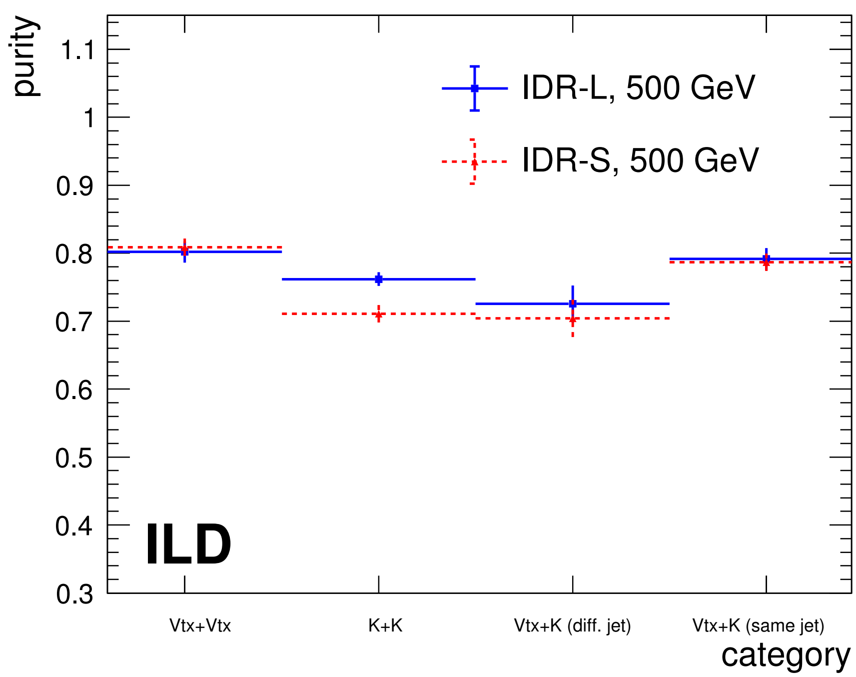

Figure 9: Purity of the different methods

Afb gen	0.328288	N: 1351248
Afb reco	0.338966	N: 210334
Final efficiency	31.1318%	

Table 3: l5 final efficiency and A_{fb}

Afb gen	0.328233	N: 1418738
Afb reco	0.338662	N: 219177
Final efficiency	30.8975%	

Table 4: s5 final efficiency and A_{fb}

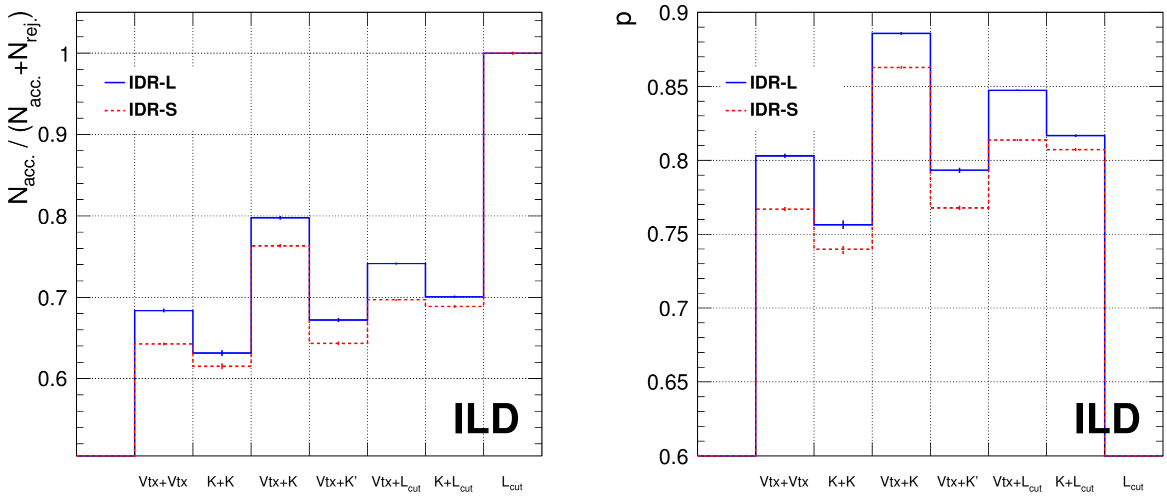

Figure 10: Calculated probability plots for $t\bar{t}$ events. Left plot shows the result of $N_{acc.}/(N_{acc.} + N_{rej.})$ and right plot shows the p values with different charge configurations.

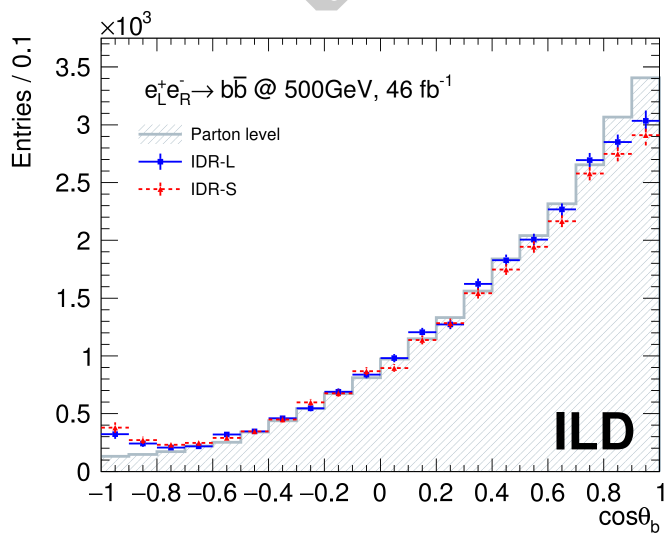

Figure 11

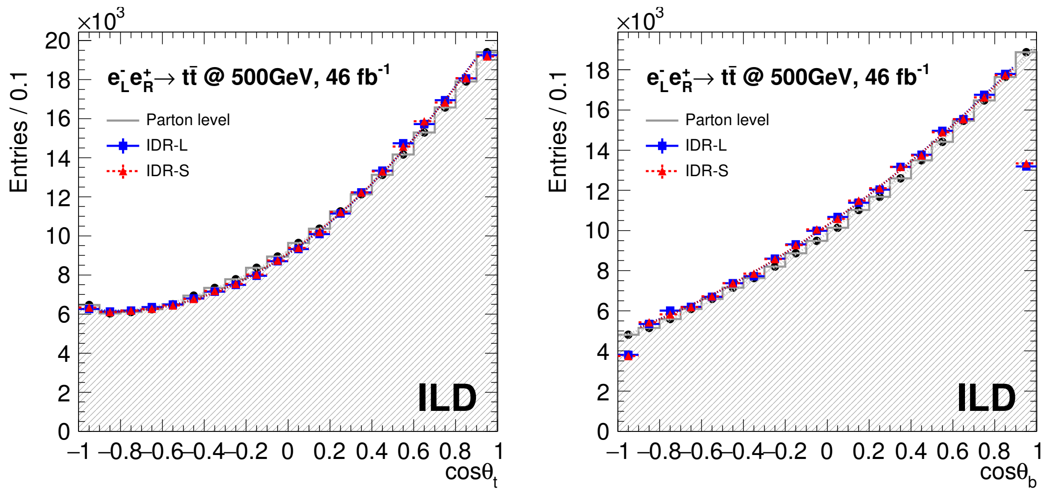

Figure 12: <u>Left:</u> *Polar angle distribution for top quark. will be on the same level.* <u>Right:</u> *Polar angle distribution for the b-quark that is issue of the top quark decay. The distributions for IDR-S is normalized to the one for IDR-L so that both histograms will be on the same level.. Distributions for IDR-S are normalised to the one for IDR-L so that both histograms*

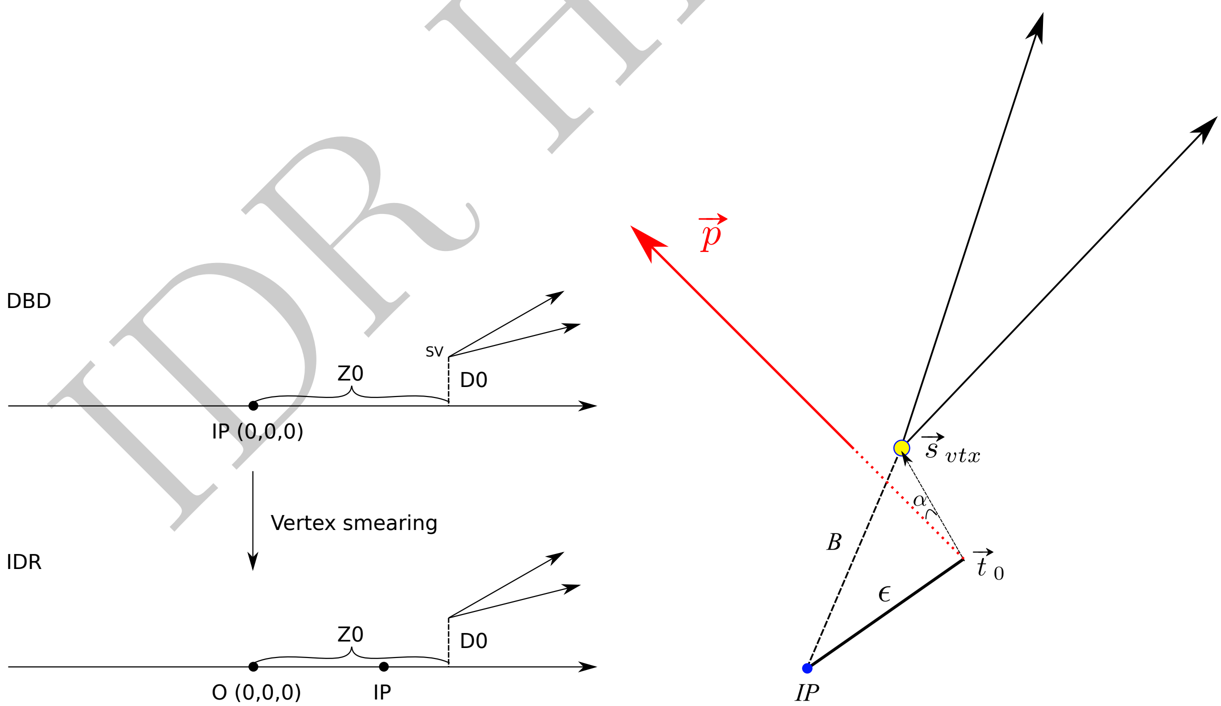

Figure 13: Left is